Serpentinization of Koçali Ophiolite in the Southeast Anatolian Orogenic Belt (Turkey)

A. Feyzi Bingöl [a*] and Melahat Beyarslan [a]

[a] *Department of Geological Engineering, Firat University, Elazığ, Türkiye.*

Authors' contributions

This work was carried out in collaboration between both authors. Both authors read and approved the final manuscript.

Article Information

Original Research Article

ABSTRACT

The Koçali ophiolite is a part of the Southeast Anatolian Orogenic Belt ophiolites. The Koçali ophiolite is represented by serpentinized mantle peridotites, gabbros, sheeted diabase dykes and basalts. They are later intruded by arc-granitoids. The serpentinized mantle peridotites consist of relics of olivine and orthopyroxene + serpentine minerals (lizardite + chrysotile + brucite) + Cr-spinel ± carbonate minerals. Two types of serpentine mineralogies and textural relationships are observed. They are: 1- lizardite mesh-textured vein networks with relict olivine cores, 2) bastite texture with serpentinization of orthopyroxene. The high LOI values (8.1 to 16.01%) indicate high degrees of serpentinization. Relatively low Al_2O_3/SiO_2 (<0.03), generally high MgO/SiO_2 (between0,86 to1,26), high MgO (>35 wt%), low Al_2O_3 (<1.2 wt%) and high Mg# values (88 to 90) indicate that the protoliths underwent significant partial melting. The serpentinites are depleted in REE concentrations compared to chondrite values. HREE less depleted than LREE. They revealed generally a small decrease from LREE to MREE (La/Sm= 2,636263 in average,) and a progressive enrichment from MREE to HREE (Sm/Lu=0,466771 in average). The overall depleted bulk concentrations in REE compositions are consistent with high melt extraction is expected for fore-arc/mantle wedge serpentinites.

_____

Corresponding author: Email: afbingol@gmail.com;

Keywords: Serpentinite; mantle peridotite; ophiolite; Koçali.

1. INTRODUCTION

Serpentinites, which are hydrated ultramafic rocks, and their serpentinization processes have attracted much attention over the last three decades due to their features in determining their tectonic setting and their economic importance. It has been suggested that the occurrence of serpentinites, particularly in subduction zones, may have important implications for the Earth's dynamic and global geochemical cycle [1,2]. The serpentinization of mantle peridotites is an important process with implication for the geochemical cycle of volatiles [3,4]. Serpentinization occurs at seafloor and continues during subduction. It is also produced in the mantle wedge/forearc environments. Ophiolites cropping out in orogenic belts consist of a crustal section and underlying mantle peridotites. Mantle peridotites preserve a record of lithospheric alteration at depths, despite emplacement and uplift [5]. Previous studies on the serpentinites [6-23] have shown important diversities of composition between abyssal, forearc/mantle wedge and subduction serpentinites.

The aim of this study is to determine the geotectonic environment of the serpentinization by examining the geochemical properties of the mantle peridotites of the Koçali Ophiolite, which is the most serpentinized among the Southeast Orogenic Belt ophiolites.

2. GEOLOGICAL OUTLINE

The Southeast Anatolian Orogenic Belt (SEAOB) forms a belt over 1000 km in length from Iskenderun Bay to triple joinction of Türkiye-Iran-Irak.

The Southeast Anatolian Orogenic Belt separated by the Southeast Anatolian Thrust Belt from the Arabian Plate. It can be divided into the Neoproterozoic to Early Triassic Metamorphic Massifs (Bitlis-Pütürge), Late Cretaceous Ophiolites and arc related magmatics, Middle Eocene Maden Complex, Late Cretaceous to Late Miocene sedimentary units. The relationships between them are mostly tectonic. There are four important tectonic periods in the region. They are 1) Tectonic events related to Cadomian orogeny, 2) Late Cretaceous tectonic events, 3) Late Eocene-Early Miocene tectonic events, and 4) Neotectonic period.

The Southeast Anatolian ophiolites are a collective name of the Kızıldağ, Koçali, Guleman, Ispendere, Kömürhan, Gevaş, Cilo, and other unnamed ophiolite fragments exposed in the Southeast Anatolian Orogenic Belt (Fig. 1). They are usually in tectonic contact with the other units and some of them have been intruded by Late Cretaceous granitic rocks, and are covered by younger sediments.
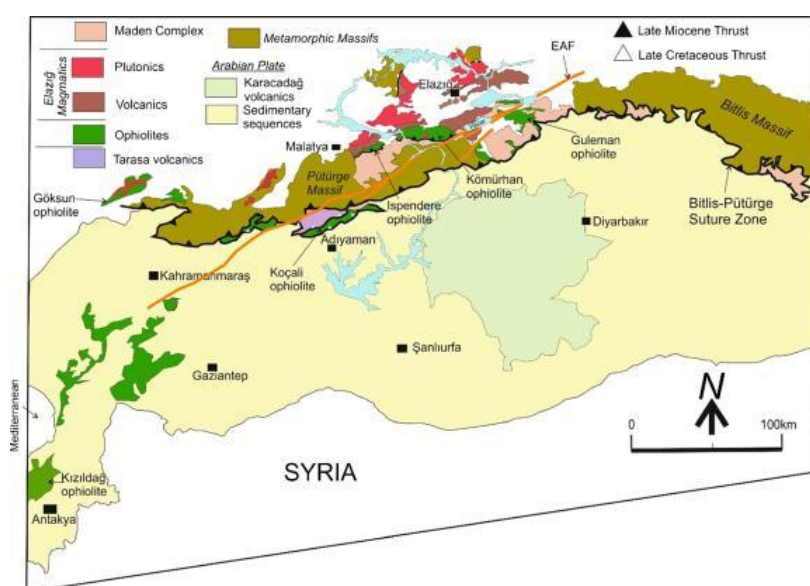
Fig. 1. Distribution of the ophiolites and arc-type igneous rock in the Southeast Taurus [from 24]
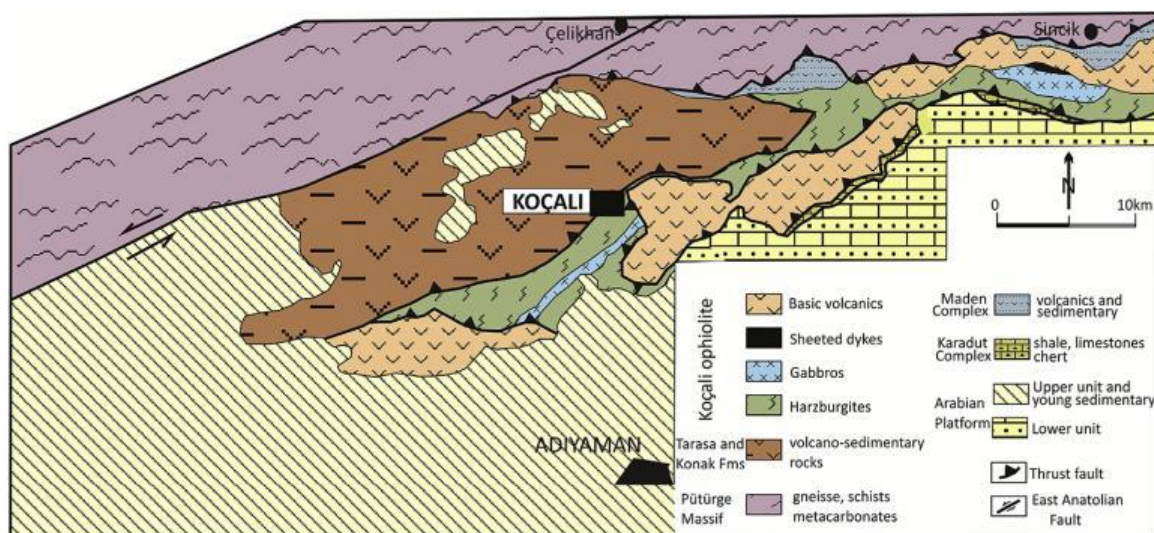
Fig. 2. Simplified geological map of the study area [from 28]

2.1. The Koçali Ophiolite

The Koçali ophiolite corresponds to the Kale Formation of the Koçali Complex, which consists of the Tarasa, Konak and Kale formations [25-27].

The main lithology of the Koçali ophiolite is mainly residual harzburgite and crustal rocks (Fig. 2). The age of the Koçali Ophiolite is constrained to 92.6±1 Ma by U-Pb dating of zircon in plagiogranite that cut the upper section of the ophiolite [24]. The Koçali ophiolite has been suggested to have mainly formed in a SSZ setting [24,28].

3. METHODOLOGY

Forty representative peridotite samples of the Koçali ophiolitic massif were collected for petrographic and geochemical study. Also, 5 samples were collected from Kızıldağ and 5 samples from Gulemann ophiolites for comparison. After petrographical investigations, 20 (13 from Koçali, 4 from Kızıldağ and 3 from Guleman) samples with a high degree of serpentinization were prepared for geochemical analysis. Serpentine mineral species were identified under polarizing microscope and confirmed by XRD with a detector SC-70, operating at 40kV and 15mA at Munzur University (Tunceli-Türkiye).

Bulk-rock major contents were determined by both X-Ray fluorescence (XRF) and atomic emission spectroscopy ICP-AES, and trace element contents were determined by Ionic Leach methods at ALS Geochemistry, North Vancouver, Canada. Prior to shipping to ALS, samples were trimmed to remove weathered surfaces. Samples were crushed passing through a 2 mm mesh and pulverized in the laboratories of the Geological Engineering Department of Firat University before being sent to the ALS. To calculate the loss of ignition (LOI), 2 g of sample powder was reweighed after heating at $1000^{o}C$ for 2 hours and cooling, the difference with the initial weight recorded as percent LOI. 100 mg of powdered samples was added to lithium metaborate/lithium tetraborate, mixed well and fused in a furnace at $1000^{o}C$. Sample taken from the furnace was then dissolved in 4% HNO_3/2%HCl. This solution was then analyzed by ICP-AES (ALS Geochemistry method ME-ICP06). Since the contents of trace elements and rare earth elements are very low, the Ionic Leach method of ALS (ME-MS23 method) was used. B content was detected by Aqua Regia (ME-MS42 method).

4. PETROGRAPHICAL AND MINERA-LOGICAL CHARACTERISTICS

Some of the studied samples were previously examined by Beyarslan et al. [29], Beyarslan [24] and Rizeli [30], in addition, the majority of the samples are described in this study based on heavily serpentinized peridotite thin sections from Koçali Ophiolite. The peridotites in the study area were mostly highly serpentinized. Heavily serpentinized specimens were investigated for the first time in this study. In addition, all of the

peridotites were weathered by seawater. The serpentinites have a mineral assemblage of lizardite+ chrysotile+olivine+magnetite±brucite± chlorite±carbonate. Clinopyroxene (<2%) is usually formed as exsolution lamellae in orthopyroxene crystals. Modal analyses of peridotites based on their primary mineral (olivine+orthopyroxene) abundances indicate that harzburgite is predominant and dunite is subordinate. Dunite increases proportionally towards the upper levels of the mantle peridotites. Olivine occurs as small grains and is replaced by lizardite at cracks and grain boundaries (Fig.3A and B).Examined peridotites samples always contain chromian spinel. In low-grade serpentinized dunite, chromian spinel

occurs as euhedral-anhedral crystals, while in harzburgite it occurs as anhedral crystals. In highly serpentinezed samples, chromian spinel is partly replaced by magnetite along the rim of serpentine minerals. A certain number of carbonate-bearing veins with centimeter widths can be observed in the serpentinite.

There are two types of alteration mineralogies and textural relationships: 1- lizardite mesh-textured vein networks with relict olivine cores, 2) bastite texture with serpentinization of orthopyroxene. Mesh-textured serpentine veins with fresh olivine cores occur in all samples. while bastite texture occurs in harzburgitic samples (Fig.3).

4.1 Serpentine Minerals

The rocks of mantle peridotites contain two texturally and crystallographically distinct serpentine mineral types all of which can co-exist with in a single sample. Serpentine types were determined by polarizant microscopy and confirmed by XRD (Figs.3, 4 and 5). In the serpentinized peridotite samples examined, lizardite, chrysotile and brucite are observed as serpentine minerals. In addition, carbonate veins are also observed. Cross-cutting relationships indicate that lizardite formed first, followed by chrysotile.
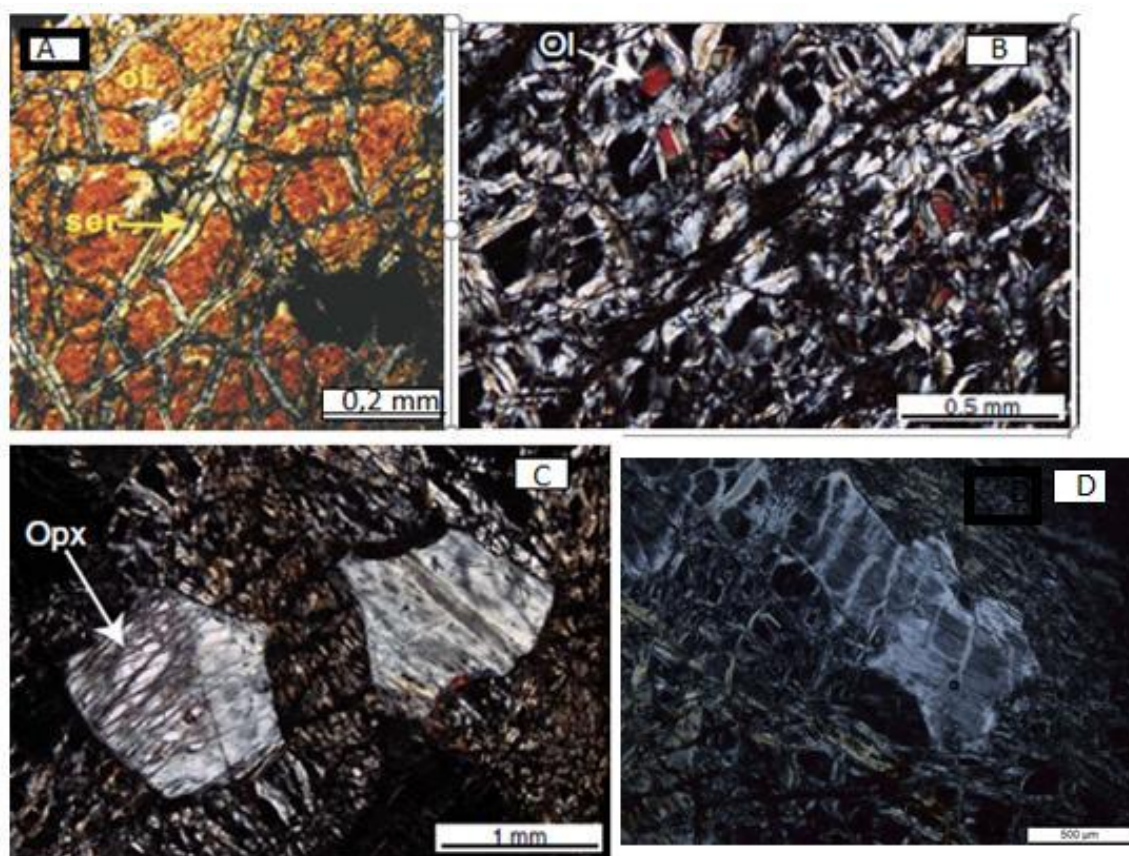
Fig. 3. (A) Mesh texture with cores of relict olivine (ol) and rims of serpentine (ser) in dunite, (B) Mesh texture of chrysotile and/or lizardite in peridotite (C) Bastite texture filled with chrysotile and/or lizardite after orthopyroxene in Harzburgite (D) Chrysotile vein in dunite
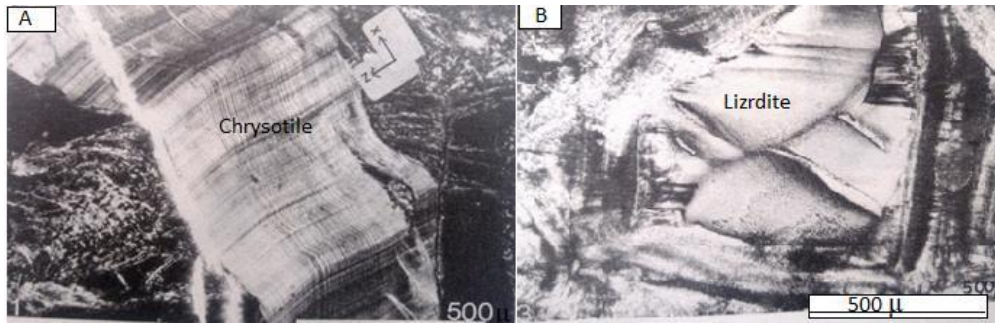
**Fig. 4. A) Chrysotile fibers that cut all minerals in thin section (PL 50x)
B) Lizardite at the core of a mesh texture formed by chrysotile (PL 80x)**
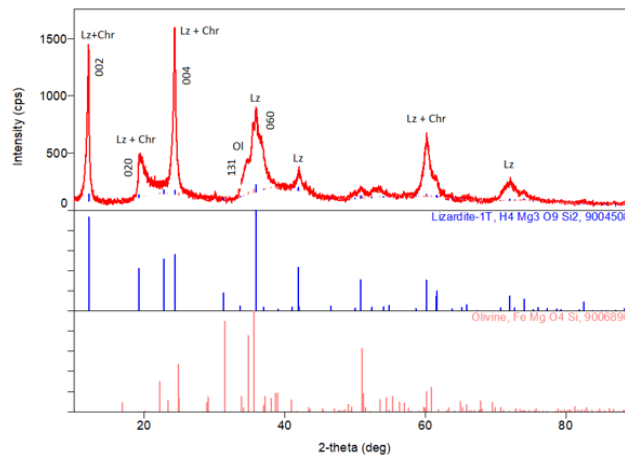
**Fig. 5. Selected bulk-rock X-ray diffraction (XRD) spectra: lizardite (L)
and chrysotile (C) are identified in samples from Koçali Ophiolite**

Chrysotile: Chrysotile is a rare species. It forms veins with thicknesses varying in the range of 0.1- 1cm, cutting lizardite and other minerals. Chrysotile is fibrous and the fibers are arranged perpendicular to the edges of the veins (Fig. 4A). sometimes the middle part of these veins is commonly marked by a sort of magnetite suture.

Lizardite: Lizardite is a common mineral in serpentinized dunite and partially serpentinized harzburgite samples. It occurs as massive grains between olivine relics and sometimes surrounded by chrysotile (Fig. 4B) in both dunite and harzburgite. It occures at the core of mesh textures in the highly serpantinized samples.

Bastite: Bastite is formed by the serpentinization of orthopyroxene (Fig. 3C).

5. RESULTS

Results of whole rock analyses are given in Table 1. The LOI (loss on ignition; wt.%) values of the examined serpentine samples ranged from 8.1 to 16.01% indicating high degrees of serpentinization and are consistent with the excessive serpentinization observed in petrographic examinations (Table 1). Relatively low Al_2O_3/SiO_2 (<0.03) and generally high MgO/SiO_2 (between 0,86-1,26) of samples studied are consistent with a refractory protolith, [10]. Bulk-rock Mg# [(100×(MgO/40.30)] / [(MgO/40.30)+(Fe_2O_3/71,85)] is high ranging between 88 to 90 and no significant variation from harzburgites to dunites is observed. CaO is low (less than 1 wt%) for almost all samples (except for three samples). When the samples are plotted on the LOI versus MgO (anhydrous forms; wt.%) diagram developped by Deschamps et al. (2013), they mostly fall into the chrysotile/lizardite area (Fig. 6).

REE compositions are variable, but remain relatively depleted. The studied serpentinites are depleted in LREE concentrations compared to chondrite values. HREE less depleted than LREE (Fig. 7). They have smaller positive Eu anomalies. They generally a small decrease from LREE to MREE (La/Sm= 2,636263 in average,) and a progressive enrichment from MREE to HREE (Sm/Lu=0,466771 in average).

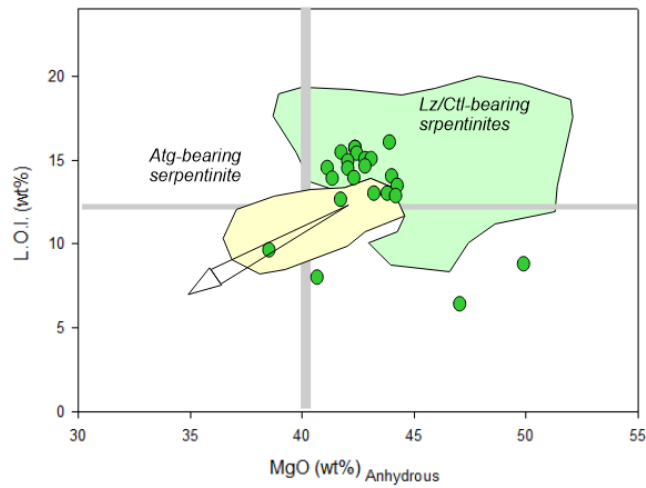**Fig. 6. LOI (loss on ignition; wt.%) versus MgO (anhydrous forms; wt.%) diagram. for serpentinites [serpentinite fields from 8]**
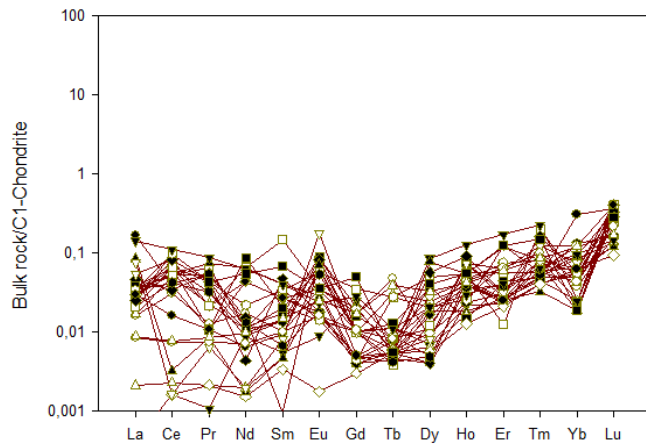

Fig. 7. Chondrite-normalized REE patterns for serpentinites from Koçali ophiolite. Chondrite values are from Sun&McDonough [31]
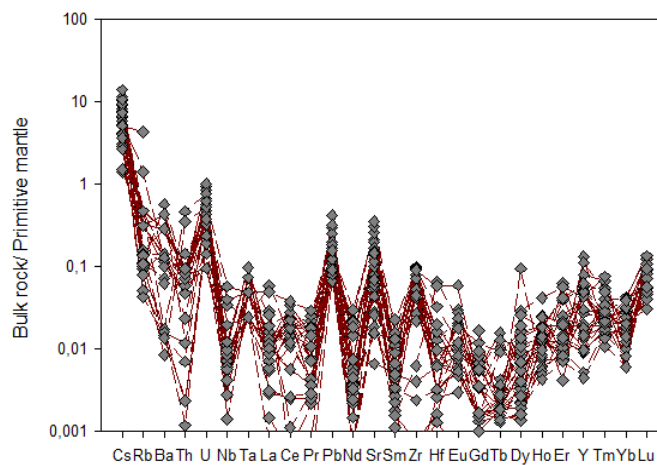

Fig. 8. Primitive mantle-normalized spider diagrams for serpentinite from the Koçali ophiolite. The primitive mantle values are from McDonough&Sun [32]

As shown in Fig. 8, the bulk-rock trace element patterns normalized to primitive mantle show large enrichments in Cs, U, Sr and Pb. In the PM normalized pattern diagram, all of the investigated serpentinites show a depletion for most incompatible elements.

Table 1. Whole-rock (%wt), trace elements and REE analyses Koçali serpentinites

Locality	Koçali (Adıyaman)							
N. No	12Kc15	17Kc15	20Kc16	24Kc16	41Kc16	15Kc18	34Kc18	51Kc18
SiO2	38,37	38,75	39,45	38,65	38,84	43,38	39,54	39,59
TiO2	0,01	0,02	0,06	0,01	0,09	0,01	0,02	0,02
Al2O3	0,36	0,68	0,69	0,48	2,12	1,12	0,56	1,17
Fe2O3	7,67	8,31	8,15	8,64	8,26	8,07	7,98	7,64
MnO	0,12	0,12	0,1	0,1	0,18	0,12	0,09	0,13
MgO	36,79	35,49	35,65	36,11	35,45	37,32	36,53	35,26
CaO	0,04	0,11	0,37	0,08	0,24	1,22	0,07	0,07
Na2O	0,02	0,01	0,01	0,01	0,02	0,02	0,01	0,01
K2O	0,01	0,01	0,01	0,01	0,01	0,01	0,01	0,01
P2O5	0,01	0,01	0,02	0,02	0,03	0,02	0,02	0,01
Cr2O3	0,359	0,486	0,265	0,503	0,481	0,423	0,305	0,433
LOI	16,01	15,7	14,9	15,1	14	8,1	14,5	15,4
TOTAL	99,97	99,95	99,96	99,96	99,95	99,94	99,95	99,95
Mg#	89,53	88,39	88,63	88,17	88,44	89,18	89,08	89,16
Al2O/SiO2	0,0094	0,0175	0,0175	0,0124	0,0546	0,0258	0,0142	0,0296
B	7,23	56,21	35,18	42,12	37,26	62,43	52,13	61,45
Li	0,25	3,12	2,65	0,81	4,56	6,21	5,13	0,89
Ba	1	3	4	2	1	0,8	1	0,9
Cs	0,065	0,011	0,083	0,024	0,041	0,033	0,051	0,032
Ga	2,4	1,9	1,8	0,8	2,8	1,7	1,3	1,3
Hf	0,001	0,005	0,004	0,002	0,001	0,002	0,001	0,003
Nb	0,006	0,008	0,002	0,001	0,004	0,008	0,005	0,004
Rb	0,09	0,2	0,07	0,1	0,3	0,09	0,06	0,2
Sr	1,1421	1,3321	4,5224	1,1653	4,1823	1,6341	1,6701	2,1327
Th	0,002	0,001	0,007	0,005	0,004	0,004	0,007	0,006
V	46	55	46	39	47	58	32	46
Zr	0,6	0,9	0,89	0,5	0,47	0,6	1,11	0,3
Y	0,2114	0,2341	0,6011	0,1243	0,2545	0,3621	0,5142	0,0627
La	0,04	0,0038	0,005	0,004	0,006	0,007	0,011	0,007
Ce	0,024	0,019	0,026	0,03	0,06	0,032	0,021	0,04
Pr	0,001	0,0012	0,003	0,0021	0,004	0,006	0,0051	0,001
Nd	0,003	0,008	0,004	0,005	0,0052	0,0051	0,007	0,02
Sm	0,0014	0,0015	0,0021	0,003	0,0026	0,005	0,002	0,004
Eu	0,005	0,002	0,004	0,0034	0,005	0,0032	0,0046	0,002
Gd	0,0041	0,0035	0,0021	0,002	0,0032	0,007	0,002	0,004
Tb	0,0002	0,0017	0,0004	0,0011	0,0003	0,001	0,00022	0,00021
Dy	0,0051	0,0021	0,0017	0,006	0,0027	0,012	0,014	0,0024
Ho	0,0023	0,0024	0,0012	0,0021	0,0041	0,003	0,002	0,0013
Er	0,004	0,0041	0,0036	0,0037	0,0043	0,002	0,005	0,03
Tm	0,0012	0,002	0,001	0,0018	0,0011	0,005	0,004	0,002
Yb	0,05	0,006	0,009	0,003	0,004	0,007	0,009	0,004
Lu	0,009	0,004	0,003	0,008	0,0067	0,006	0,007	0,01
Ta	0,001	0,001	0,003	0,002	0,001	0,004	0,002	0,003
Pb	0,03	0,008	0,012	0,007	0,0054	0,021	0,018	0,008
U	0,01	0,012	0,02	0,014	0,018	0,01	0,002	0

* from Rizeli 2021
(n.d. = not determined)

Table 1 continued..........

Locality	Koçali (Adıyaman)							
N. No	16Kc19	25Kc19	32Kc19	34Kc19	42Kc19	AK10*	AK11*	47Kc19
SiO2	39,29	40,15	39,7	40,05	40,03	38,4	38,58	40,04
TiO2	0,01	0,01	0,01	0,01	0,01	n.d	n.d	0,01
Al2O3	0,49	0,65	0,57	0,6	0,72	0,9	0,39	0,82
Fe2O3	8,22	8,07	7,51	8,03	8,28	7,91	8,33	7,79
MnO	0,1	0,07	0,12	0,06	0,12	0,11	0,09	0,12
MgO	35,77	36,2	36,51	37,46	35,1	38,2	37,84	35,77
CaO	0,04	0,06	0,04	0,06	0,45	0,41	0,04	0,25
Na2O	0,02	0,01	0,01	0,01	0,01	n.d	n.d	0,01
K2O	0,01	0,01	0,01	0,01	0,01	n.d	n.d	0,01
P2O5	0,02	0,02	0,03	0,01	0,02	0,02	n.d	0,02
Cr2O3	0,333	0,421	0,446	0,425	0,505	0,38	0,39	0,365
LOI	15,4	14	14,8	13	14,4	12,8	13,4	14,5
TOTAL	99,95	99,95	99,96	99,96	99,95	99,11	99,06	99,95
Mg#	88,58	88,89	89,66	89,27	88,31	89,59	89,01	89,11
Al2O/SiO2	0,0125	0,0162	0,0144	0,0150	0,0150	0,0234	0,0101	0,0205
B	72,12	6,43	5,89	9,11	29,78	n.d	n.d	6,47
Li	7,21	5,34	9,42	0,96	0,73	n.d	n.d	2,34
Ba	0,8	3	1	3	2	0,1132	0,1005	2
Cs	0,046	0,051	0,012	0,053	0,024	0,023	0,032	0,083
Ga	1	0,8	0,8	1,6	0,7	n.d	n.d	1,2
Hf	0,001	0,001	0,002	0,001	0,002	0,0008	0,0005	0,005
Nb	0,002	0,006	0,003	0,008	0,007	0,0052	0,0043	0,003
Rb	0,1	0,2	0,2	0,2	0,3	0,0325	0,027	0,2
Sr	1,2703	0,5894	0,3237	1,4952	3,5214	3,5144	0,5472	3,0121
Th	0,004	0,005	0,007	0,006	0,007	0,0001	0,0002	0,008
V	34	46	39	39	44	n.d	n.d	38
Zr	0,8	1,1	0,6	0,5	1,06	0,0037	0,0085	1,02
Y	0,0714	0,0453	0,0627	0,0411	0,1375	0,1945	0,0238	0,2153
La	0,008	0,013	0,007	0,008	0,008	0,001	0,0005	0,007
Ce	0,034	0,05	0,04	0,032	0,041	0,001	0,0014	0,01
Pr	0,007	0,002	0,003	0,005	0,004	0,0001	0,0002	0,001
Nd	0,03	0,02	0,005	0,006	0,01	0,004	0,0009	0,02
Sm	0,006	0,004	0,002	0,001	0,005	0,0008	0,0007	0,004
Eu	0,0016	0,0009	0,003	0,001	0,0008	0,0005	0,0018	0,001
Gd	0,0008	0,001	0,002	0,001	0,0009	0,0049	0,0009	0,001
Tb	0,00016	0,0002	0,00017	0,00032	0,00028	0,0003	0,0002	0,0002
Dy	0,07	0,002	0,001	0,0012	0,005	0,0211	0,0016	0,004
Ho	0,001	0,004	0,0013	0,002	0,0014	0,0069	0,0009	0,0021
Er	0,004	0,01	0,02	0,006	0,012	0,0273	0,0045	0,004
Tm	0,0008	0,003	0,0014	0,0013	0,002	0,0056	0,0012	0,0015
Yb	0,003	0,02	0,021	0,015	0,009	0,004	0,0137	0,02
Lu	0,01	0,01	0,004	0,008	0,007	0,0091	0,0034	0,01
Ta	0,004	0,001	0,002	0,004	0,001	0	0,001	0,001
Pb	0,0067	0,013	0,0064	0,014	0,023	0,0048	0,012	0,0087
U	0,003	0,002	0,021	0,008	0,013	0,007	0,004	0,012

* from Rizeli 2021
(n.d. = not determined)

Table 1 continued..........

Locality				Kızıldağ			
N. No	Kz21	Kz36	Kz41	Kz52	HA15*	15HS32-2*	HA13*
SiO2	40,05	40,03	40,04	38,59	38,13	38,05	34,68
TiO2	0,01	0,01	0,01	0,01	n.d	n.d	n.d
Al2O3	0,6	0,72	0,82	0,34	0,54	0,37	0,53
Fe2O3	8,03	8,28	7,79	8,15	7,85	8,05	8,45
MnO	0,06	0,12	0,12	0,02	0,11	0,11	0,11
MgO	37,46	35,1	35,77	41,06	42,14	39,85	43,8
CaO	0,06	0,45	0,25	0,12	0,61	0,71	0,15
Na2O	0,01	0,01	0,01	0,95	n.d	n.d	n.d
K2O	0,01	0,01	0,01	0,05	n.d	n.d	n.d
P2O5	0,01	0,02	0,02	0,03	n.d	n.d	n.d
Cr2O3	0,425	0,505	0,365	0,43	0,36	0,42	0,68
LOI	13,1	14,4	14,5	10,06	9,3	11,01	10,6
TOTAL	99,96	99,95	99,95	99,37	99,04	99,01	99
Mg#	89,27	88,31	89,11	89,98	90,54	89,82	90,24
Al2O/SiO2	0,0150	0,0180	0,0205	0,0088	0,0142	0,0097	0,0153
B	8,67	62,41	13,21	37,89	n.d	n.d	9,89
Li	0,92	2,57	8,65	8,65	n.d	n.d	2,69
Ba	3	2	2	0	0,1119	0,4376	0,0961
Cs	0,058	0,029	0,084	0,041	0,11	0,042	0,021
Ga	1,6	0,7	1,2	1,4	n.d	n.d	n.d
Hf	0,001	0,002	0,005	0,01	0,001	0,0061	0,0019
Nb	0,008	0,007	0,003	0	0,0087	0,0284	0,0139
Rb	0,2	0,3	0,2	0,76	0,091	0,0865	0,068
Sr	1,4764	3,5034	3,2014	3,0641	0,9247	0,3277	0,1394
Th	0,006	0,007	0,008	0	0,001	0,0122	0,0006
V	39	44	38	37	n.d	n.d	n.d
Zr	0,5	1,06	1,034	1,012	0,0268	0,2443	0,045
Y	0,0421	0,1957	0,2257	0,2867	0,0664	0,0448	0,0672
La	0,008	0,008	0,007	0	0,002	0,0336	0,0021
Ce	0,01	0,06	0,01	0	0,0045	0,0675	0,0047
Pr	0,005	0,004	0,001	0,004	0,0007	0,0081	0,0008
Nd	0,006	0,01	0,02	0,025	0,0033	0,029	0,0045
Sm	0,001	0,005	0,004	0,01	0,0015	0,0059	0,0022
Eu	0,001	0,0008	0,001	0,002	0,0009	0,0013	0,0014
Gd	0,001	0,0009	0,001	0,01	0,0021	0,0056	0,0034
Tb	0,00015	0,001	0,0002	0,0002	0,0003	0,0004	0,0014
Dy	0,0012	0,005	0,004	0,01	0,0069	0,0051	0,008
Ho	0,002	0,0014	0,0021	0,003	0,0024	0,0016	0,0023
Er	0,006	0,012	0,004	0,02	0,0103	0,0066	0,0096
Tm	0,0013	0,002	0,0015	0,0037	0,0025	0,0016	0,0021
Yb	0,015	0,009	0,01	0,003	0,007	0,0157	0,0194
Lu	0,008	0,007	0,01	0,007	0,0053	0,0036	0,0042
Ta	0	0,001	0,001	0,001	0,004	0,002	0,001
Pb	0,012	0,0057	0,013	0,011	0,0091	0,0087	0,0064
U	0,012	0,009	0,011	0,013	0	0,008	0,011

* from Rizeli 2021
(n.d. = not determined)

Table 1 continued...........

Locality	Guleman (Elazığ			
N. No	G-27	MG12	G-32	G-54	EG2-1A*
SiO2	39,72	42,22	38,47	38,49	36,68
TiO2	0,01	0,04	0,01	0,01	n.d
Al2O3	1,32	2,23	0,76	0,58	0,07
Fe2O3	7,72	7,91	8,15	7,71	6,67
MnO	0,11	0,12	0,11	0,11	0,09
MgO	36,39	34,72	38,09	37,74	45,92
CaO	1,44	2,3	0,77	0,72	0,25
Na2O	0,01	0,05	0,01	0,01	n.d
K2O	0,01	n.d	0,01	0,01	n.d
P2O5	0,01	0,01	0,01	0,02	n.d
Cr2O3	0,417	0,408	0,331	0,363	0,37
LOI	12,6	9,7	13,1	14,01	8,8
TOTAL	99,95	99,95	99,96	99,96	98,85
Mg#	89,37	88,67	89,28	89,72	92,47
Al2O/SiO2	0,0332	0,0528	0,0198	0,0151	0,0019
B	29,47	14,2	32,14	12,75	n.d
Li	0,98	3,27	7,26	4,65	n.d
Ba	0,7	0,12	0,5	0,9	0,1115
Cs	0,073	0,074	0,041	0,061	0,092
Ga	1,4	2,2	1	0,7	n.d
Hf	0,003	0,02	0,002	0,002	0,0004
Nb	0,001	0,006	0,041	0,003	0,0244
Rb	0,2	0,3	0,07	0,2	0,064
Sr	5,5231	2,4102	6,4427	7,5012	3,1025
Th	0,004	0,04	0,008	0,007	0,0002
V	52	58	35	29	n.d
Zr	1,037	0,07	1,033	1,056	0,0063
Y	0,2254	0,2631	0,0901	0,0816	0,0203
La	0,009	0,02	0,005	0,006	0
Ce	0,04	0,002	0,04	0,05	0,001
Pr	0,001	0,0008	0,002	0,004	0,0002
Nd	0,04	0,0008	0,03	0,002	0,0007
Sm	0,003	0,0007	0,004	0,007	0,0005
Eu	0,0008	0,004	0,002	0,001	0,0001
Gd	0,002	0,001	0,002	0,0008	0,0006
Tb	0,00046	0,0002	0,00014	0,0002	0,0002
Dy	0,009	0,019	0,003	0,001	0,0014
Ho	0,0008	0,003	0,0031	0,0025	0,0007
Er	0,007	0,019	0,009	0,012	0,0034
Tm	0,0012	0,002	0,0014	0,002	0,001
Yb	0,008	0,01	0,007	0,01	0,01
Lu	0,009	0,003	0,01	0,008	0,0023
Ta	0	0	0,002	0,002	0,001
Pb	0,011	0,0057	0,0078	0,0069	0,011
U	0,014	0,016	0,013	0,008	0,005

* from Rizeli 2021
(n.d. = not determined)

6. DISCUSSION

The protolith of serpentinites in orogenic zones represent either residual mantle peridotites or ultra-mafic cumulates. They comprise abyssal slab peridotites and mantle wedge peridotites [8,33]. The protolith of the Koçali serpentinites have primary mantle minerals, such as olivine and orthopyroxene relicts. In addition, there are generally anhedral chromian spinel crystals,

however, some samples contain euhedral chromite crystals. These relic minerals and chrome spinel crystals indicate that the protoliths of serpentinites are mantle peridotite harzburgite and dunite. Koçali serpentinite samples are the most refractory serpentinites, with high MgO (>35 wt%) and low Al_2O_3 (<1.2 wt%; Table 1). They contain high Mg# values ranging between 88 to 90. Their high Mg#, low Al_2O_3 values, low Al_2O_3/SiO_2 (<0.03) and generally high MgO/SiO_2 (0.86;1.26) indicate that the protoliths underwent significant partial melting. Major element compositions of forearc/mantle wedge serpentinites and abyssal slab serpentinites show significant overlap. However, forearc/mantle wedge serpentinites are more refractory than the latter [8,34]. The abyssal slab serpentinites exhibit lower MgO and higher FeO, SiO_2 and Al_2O_3 contents compared to the forearc/mantle wedge serpentinites. Moreover abyssal slab serpentinite has overall lower Mg# and MgO/SiO_2, but higher Al_2O_3/SiO_2 than forearc/wedge serpentinite. The Koçali Ophiolite serpentinites have low TiO_2 (usually 0.1% or less). Ti concentration is a reliable indicator for the determination of protoliths of serpentinites (bulk-rock Ti concentrations: mantle wedge serpentinites 2-50ppm, abyssal slab serpentinites: 10-130ppm, subducted serpentinites >50ppm. These values indicate that the Koçali ophiolite serpentinites are consistent with the mantle wedge serpentinites.

The studied serpentinites are depleted in REE concentrations compared to chondrite values. HREE are less depleted than LREE (Fig. 7). They have smaller positive Eu anomalies. They generally a small decrease from LREE to MREE (La/Sm= 2,636263 in average,) and a progressive enrichment from MREE to HREE (Sm/Lu=0,466771 in average). The overall depleted bulk concentrations in REE compositions are consistent with high melt extraction is expected for fore-arc/mantle wedge serpentinites. Kodolányi et al. [13], who made a compilation about the geochemical properties of the abysal serpentinite and the mantle wedge serpentinites indicate that serpentinites from mid-oceanic ridges have overall higher REE concentrations than those from mantle wedges.

When the samples are plotted on Rb vs. Cs and Li vs. Cs diagrams of Peters et al. [35], all samples fall into forearc serpentinites area (Fig. 9A and B). Discriminative element enrichment ratios are Rb:Cs < 10, and Li:Cs < 100. The samples fall into the mantle wedge area

on Sr vs. Yb, Nb vs. La and La/Yb vs. Yb diagrams of Deschamps et al. [8] (Fig. 10). The differences of names in these diagrams come from the nomenclature between the two groups of authors. Deschamps et al. [8] distinguish serpentinites as abyssal, subducted and mantle wedge-forearc serpentinites and use mantle wedge serpentinite areas in their discriminant diagrams. Whereas, Peters et al. [35] use the term forearc serpentinites rather than mantle wedge serpentinites for shallow hydrated mantle wedge and forearc/accretionay wedge serpentinites.

There is no correlation between REE contents and LOI. This suggests that the mantle protolith might preserve the REE signature [19,20].

Bulk rock/Primitive mantle spider diagrams are characterized by Cs, Rb, U, Ta, Pb, Sr and Zr enrichments. The enrichments of Pb and Sr are similar to those of abyssal serpentinites, however, Cs and Rd enrichments are not observed in abyssal contexts.

The trace elements (except for of Cs, Rb) are depleted compared to primitive mantle (Fig. 8). The samples are characterized by low HREE (e.g. Yb_N=0.006-0.1). There are enrichments in LREE relative to MREE. The samples are LREE depleted to HREE (La_N/Yb_N=0.026-0.95) except for samples 41Kc16, 51Kc18, 16Kc19 (La_N/Yb_N= 1.07, 1.25, 1.91 respectively). The enrichments in these LRE elements are considered to be the result of the melt/rock interaction with the percolation of these elements in the depleted mantle [3,36,37]. The serpentinite samples display no to slight Eu anomalies. The low trace element concentrations are characteristic features of mantle wedge serpentinites. Low concentrations are due to high degrees of partial melting of mantle peridotites. All these data show that the compositions of the examined samples are similar to the compositions of mantle wedge/forearc rocks [7,19-21]. The Koçali serpentinites are enriched in Cs, Rb, Ba, Sr, Pb. These enrichment probably reflect the elevated concentrations of these elements in the mantle wedge hydrating fluids [8,38-44].

In the studied samples, the lizardite, chrysotile and brucite are reported with varying proportions There is no antigorite. The absence of antigorite, only the presence of lizardite and chrysotile+brucite in different proportions indicate that serpentinization occurs at low temperatures. The formation of lizardite and chrysotile are started at temperature <350°C [45] and

are stable under temperatures of 400-440°C [46]. Alt and Shanks [47] estimate that serpentinization took place within the mantle wedge over temperatures of about 300–375°C, and that percolating fluids were released from the slab at a temperature lower than 200 °C.

Fig. 11 show the stability field of serpentine minerals and the geotectonical model of the formation of Koçali ophiolite and mantle wedge serpentinites. As seen in Fig. 11, lizardite+chrysotile is stable <440°C.
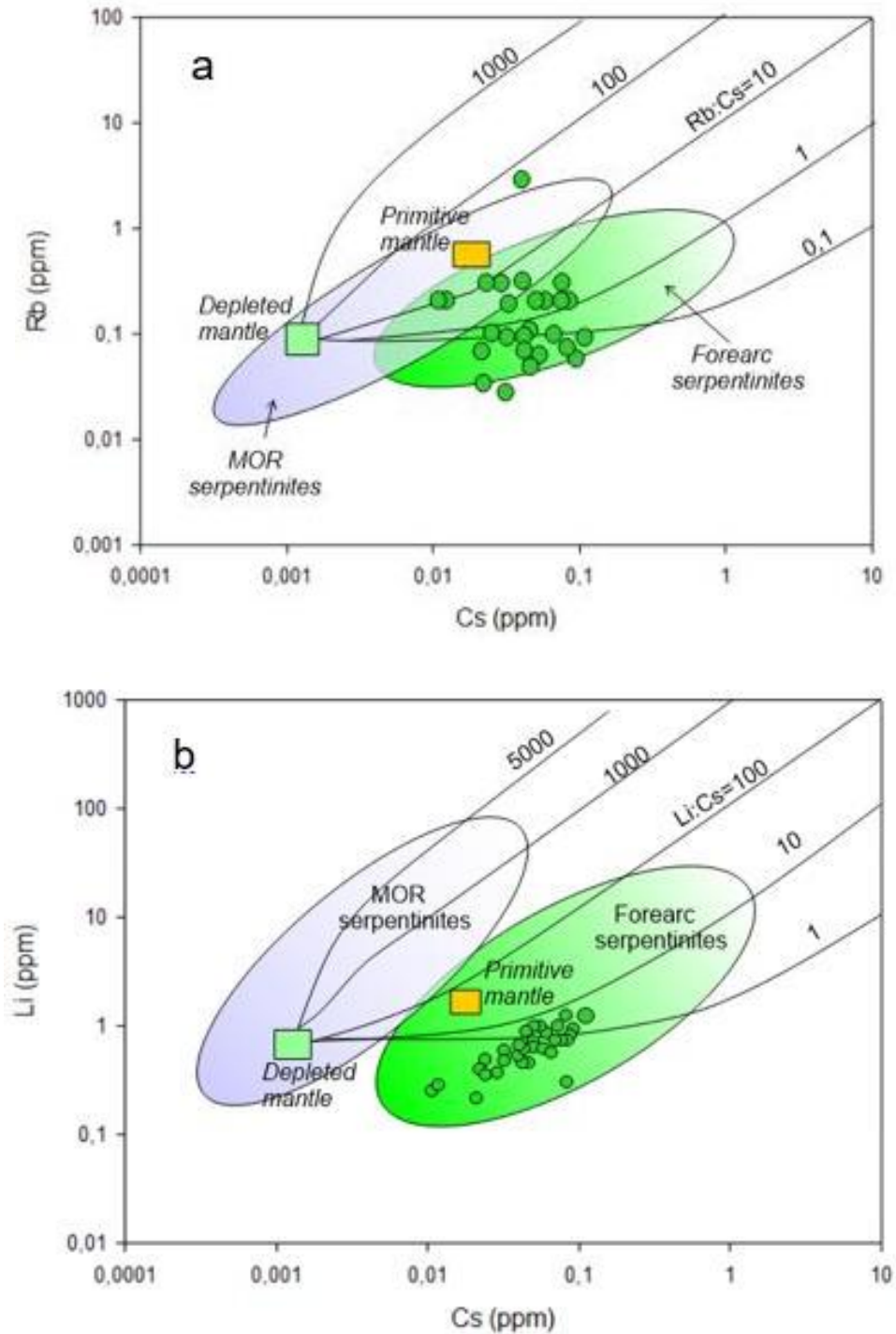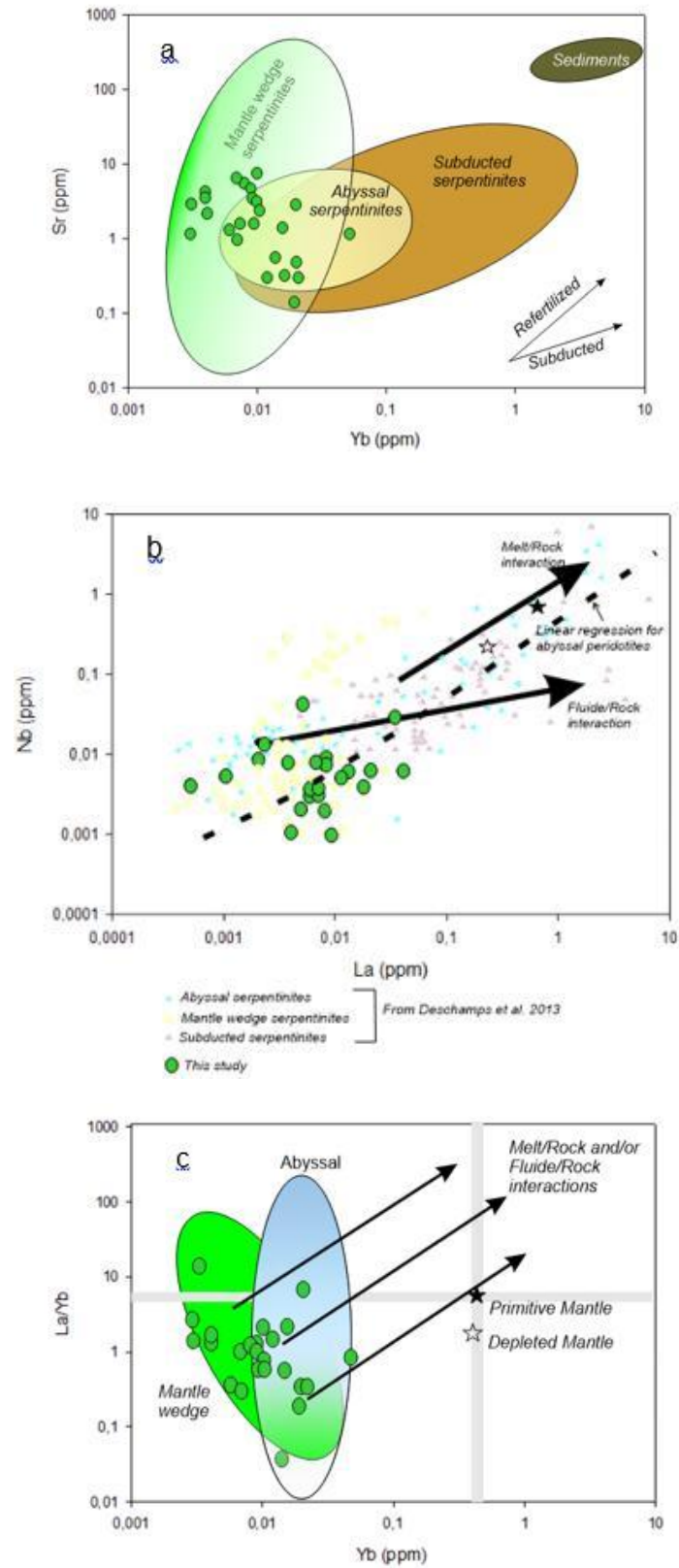

Fig. 9. Element discrimination for (a) Rb vs Cs and (b) Li vs Cs for whole rock of the Koçali serpentinites. MOR serpentinites and forearc serpentinites [35], depleted mantle [18]

Fig. 10. Element discrimination for (a) Sr vs Yb, (b) Nb vs La and (c) La/Yb vs Yb for whole rock of the Koçali serpentinites. MOR serpentinites and forearc serpentinites [35], depleted mantle [18]
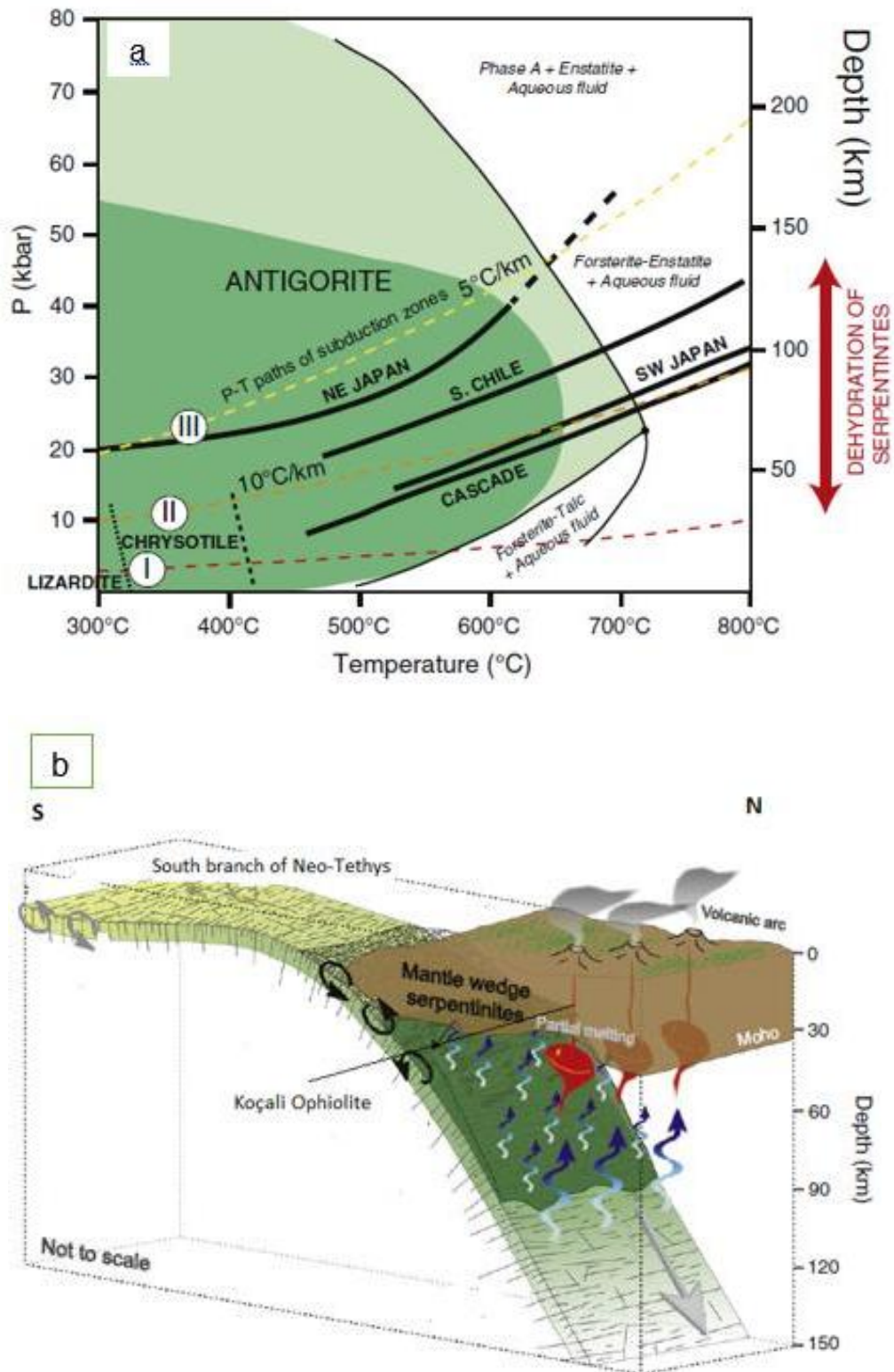
Fig. 11. (a) Stability fields of serpentine minerals after Deschamps et al. [8] b.) Schematic sketch illustrating the formation of Koçali ophiolite and mantle serpentinites

7. CONCLUSION

Koçali ophiolite, located in the Southeast Anatolian Orogenic Belt, consists of mantle rocks and crustal rocks. The LOI (loss on ignition; wt.%) values of the examined serpentine samples ranged from 8.1 to 16.01% indicating high degrees of serpentinization. Petrographical and XRD data indicate that the serpentine minerals are lizardite+chrysotile±brucite. Major and trace element compositions are consistent with a refractory protolith. The REE compositions are consistent with high melt extraction is expected for fore-arc/mantle wedge serpentinites.

ACKNOWLEDGMENTS

COMPETING INTERESTS

Authors have declared that no competing interests exist.

REFERENCES

1. Hattori KH, Guillot S. Volcanic fronts form as a consequence of serpentinite dehydration in the forearc mantle wedge. Geology. 2003;31(6):525–528.
2. Hilairet N, Reynard B, Wang Y, Daniel I, Merkel S, Nishiyama N, Petitgirard, S. High-pressure creep of serpentine, ınterseismic deformation, and ınitiation of subduction. Science. 2007;318(21): 1911-1913.
3. Holland G, Ballentine CJ. Seawater subduction controls the heavy noble gas composition of the mantle. Nature. 2006;441:186–191.
4. Kendrick MA, He´mond C, Kamenetsky VS, Danyushevsky L, Devey CW, Rodemann T, Jackson MG, Perfit MR. Seawater cycled throughout earth's mantle in partially serpentinized lithosphere. Nat. Geosci. 2017;10:222–228.
5. Bosch D, Jamais M, Boudier F, Nicolas A, Dautria JM, Agrinier P. Deep and high-temperature hydrothermal circulation in the Oman ophiolite - Petrological and isotopic evidence. J. Petrol. 2004;45:1181–1208.
6. Bodinier JL, Godard M. Orogenic, ophiolitic, and abyssal peridotites. Treatise on Geochemistry. In: Carlson, R.W. (Ed.), Mantle and Core. Treatise on Geochemistry,. Elsevier Science Ltd. 2003; 2:103–170.
7. Deschamps F, Guillot S, Godard M, Chauvel C, Andreani M, Hattori K. In situ characterization of serpentinites from forearc mantle wedges: Timing of serpentinization and behavior of fluid-mobile elements in subduction zones. Chemical Geology. 2010;269:262–277.
8. Deschamps F, Godard M, Guillot S, Hattori K, Geochemistry of subduction zone serpentinites: A review. Lithos. 2013;178: 96–127. Available:http://dx.doi.org/10.1016/j.lithos. 2013.05.019.
9. Douville E, Charlou JL, Oelkers EH, Bienvenu P, Jove Colon CF, Donval JP, Fouquet Y, Pricur D, Appriou P. The rainbow vent fluids (36°14′N, MAR): The influence of ultramafic rocks and phase separation on trace element content in mid-Atlantic ridge hydrothermal fluids. Chemical Geology. 2002;184;37–48.
10. Godard M, Lagabrielle Y, Alard O, Harvey J. Geochemistry of the highly depletedperidotites drilled at ODP Sites 1272 and 1274 (Fifteen-Twenty Fracture Zone, Mid-Atlantic Ridge): İmplications for mantle dynamics beneath a slow spreading ridge. Earth and Planetary Science Letters. 2008;267:410–425.
11. Hattori KH, Guillot S. Geochemical character of serpentinites associated with high- to ultrahigh-pressure metamorphic rocks in the Alps, Cuba, and the Himalayas: Recycling of elements in subduction zones. Geochemistry, Geophysics, Geosystems. 2007;8(9). Available:http://dx.doi.org/10.1029/2007GC 001594.Hilairet et al., 2007.
12. Kendrick MA, Honda M, Pettke T, Scambelluri M, Phillips D, Giuliani A. Subduction zone fluxes of halogens and noble gases in seafloor and forearc serpentinites. Earth Planet. Sci. Lett. 2013;365:86–96. Avaialble:http://dx.doi.org/10.1016/j.epsl.20 13.01.006
13. Kodolányi J, Pettke T, Spandler C, Kamber BS, Gméling K. Geochemistry of ocean floor and fore-arc serpentinites: Constraints on the ultramafic input to subduction zones. Journal of Petrology. 2012;53:235–270.
14. Marchesi C, Garrido CJ, Godard M, Belley F, Ferré E. Migration and accumulation of ultra-depleted subduction-related melts in

the Massif du Sud ophiolite (New Caledonia). Chemical Geology. 2009; 266:171–186.

15. Niu Y. Bulk-rock major and trace element compositions of abyssal peridotites: İmplications for mantle melting, melt extraction and post-melting processes beneath mid-ocean ridges. Journal of Petrology. 2004;45:2423–2458.

16. Parkinson IJ, Pearce JA. Peridotites from the Izu–Bonin–Mariana forearc (ODP Leg 125): Evidence for mantle melting and melt–mantle interaction in a suprasubduction zone setting. Journal of Petrology. 1998;39 (9):1577–1618.

17. Paulick H, Bach W, Godard M, De Hoog JCM, Suhr G, Harvey J. Geochemistry of abyssal peridotites (mid-Atlantic ridge, 15°20′N, ODP leg 209): İmplications for fluid/rock interaction in slow spreading environments. Chem. Geol. 2006;234(3–4):179–210.
Available:http://dx.doi.org/10.1016/j.chemgeo.2006.04.01123-

18. Salters VJM, Stracke A. Composition of the depleted mantle. Geochemistry, Geophysics, Geosystems. 2004;5(5).
Available:http://dx.doi.org/10.1029/2003GC000597.

19. Savov IP, Ryan JG, D'Antonio M, Kelley K, Mattie P. Geochemistry of serpentinized peridotites from the Mariana Forearc Conical Seamount, ODP Leg 125: İmplications for the elemental recycling at subduction zones. Geochemistry, Geophysics, Geosystems 2005a.;6(4).
Available:http://dx.doi.org/10.1029/2004GC000777.

20. Savov IP, Guggino S, Ryan JG, Fryer P, Mottl MJ. Geochemistry of serpentinite muds and metamorphic rocks from the Mariana forearc, ODP Sites 1200 and 778–779, South Chamorro and Conical Seamounts. In: Shinohara, M., Salisbury, M.H., Richter, C. (Eds.), Proceedings of the Ocean Drilling Program, Scientific Results. 2005b;195;1–49.

21. Savov IP, Ryan JG, D'Antonio M, Fryer P. Shallow slab fluid release across and along the Mariana arc-basin system: insights from geochemistry of serpentinized peridotites from the Mariana fore arc. Journal of Geophysical Research. 2007;112.
Available:http://dx.doi.org/10.1029/2006JB004749.

22. Schmidt K, Koschinsky A, Garbe-Schönberg D, Carvalho (de) L.M, Seifert R. Geochemistry of hydrothermal fluids from the ultramafic-hosted Logatchev hydrothermal field, 15°N on the Mid-Atlantic Ridge: Temporal and spatial investigation. Chemical Geology. 2007; 242:1–21.

23. Sutra E, Manatschal G. How does the continental crust thin in a hyperextended rifted margin? Insights from the Iberia margin. Geology. 2012;40:139–142.

24. Bingöl AF, Beyarslan M, Lin Y-C, Lee H-Y. 2018. Geochronological and geochemical constraints on the origin of the southeast Anatolian ophiolites, Turkey. Arabian Journal of Geosciences. 2018;11:569.
Available:https://doi.org/10.1007/s12517-018-3880-0

25. Perinçek D. Çelikhan-Sincik-Koçali (Adıyaman ili) alanının Jeoloji incelemesi ve Petrol Olanaklarının Araştırılması. PhD thesis (unpublished). I.Ü. Fen Fakültesi. 1978;212s.

26. Perinçek D (1979) The geology of Hazro-Korudağ, Çüngüş -Maden- Ergani-Hazar-Elazığ-Malatya region. In: Guide book, Geological Society of Turkey, Special Publications, 33.

27. Bingöl AF. Çermik Yöresinde (Diyarbakır) Koçali Karmaşığına ait Magma Kayalarının Jeokimyası ve Petrolojisi. Tübitak Yerbilim Derg. 1994;3:55–61.

28. Beyarslan M. Supra-subduction zone magmatism of the Koçali ophiolite, SE Turkey. J Afr Earth Sci. 2017;129: 390–402.

29. Beyarslan M, Bingöl AF, Rizeli ME. Koçali (Adıyaman) Ofiyolitindeki Manto Peridotitlerinin Jeokimyası (ana oksitler, iz elementler, Platin Grubu Elementler) ve petrolojisi, Project No. MF. 2014;12:35.

30. Rizeli ME. GD Anadolu Orojenik Kuşağı Ofiyolitlerinin Manto Peridotitleri Bileşimleri ve Petrolojisi: Ana Element, İz Element Jeokimyası, Mineral Kimyası ve Fe, Mg ve Os İzotopları. Unpubl. PhD Thesis, Firat University, Graduate School of Natural and Applied Sciences Elazığ (in Turkish with English abstract). 2021;205.

31. Sun SS, McDonough WF. Chemical and isotopic systematics of oceanic basalts: İmplications for mantle composition and processes. Geological Society, London, Special Publications. 1989;42(1):313–345.
Available:https://doi.org/10.1144/GSL.SP.1989.042.01.19.

32. McDonough, WF Sun, SS. The composition of the Earth. Chemical Geology. 1995;120:223–253.

33. Evans BW, Hattori K, Baronnet A. Serpentinite: What, why, where? Elements 2013;9:99–106.

34. Zhang L, Sun WD, Chen RX. Evolution of serpentinite from sea floor hydration to subduction zone metamorphism: Petrology and geochemistry of serpentinite from the ultrahigh pressure North Qaidam orogen in northern Tibet. Lithos. 2019;346-347: 105158.
Available:https://doi.org/10.1016/j.lithos.20 19.105158.

35. Peters D, Bretschera A, Johnb T, Scambelluric M, Pettke T. Fluid-mobile elements in serpentinites: constraints on serpentinisation environments and element cycling in subduction zones. Chemical Geology. 2017;466:654–666.

36. Navon O, Stolper E, Geochemical consequences of melt percolation: The upper mantle as a chromatographic column. Journal of Geology. 1987;95: 285–307.

37. Bodinier JL, Vasseur G, Vernieres J, Dupuy C, Fabries J. Mechanisms of mantle metasomatism: Geochemical evidence from the Lherz orogenic peridotite. Journal of Petrology. 1990; 31(3):597 628.
Available:https://doi.org/10.1093/petrology/ 31.3.597.

38. Bebout GE, Barton MD. Tectonic and metasomatic mixing in a subductionzone melange: İnsights into the geochemical evolution of the slab-mantle interface. Chemical Geology. 2002;187:79–106.

39. Hyndman RD, Peacock SM. Serpentinization of the forearc mantle. Earth and Planetary Science Letters. 2003;212:417–432.

40. Iwamori H. Transportation of H2O and melting in subduction zone. Earth and Planetary Science Letters. 1998;160: 65–80.

41. Scambelluri M, Müntener O, Ottolini L, Pettke TT, Vannucci R. The fate of B, Cl and Li in the subducted oceanic mantle and in the antigorite breakdown fluids. Earth and Planetary Science Letters. 2004;222:217–234.

42. Schmidt MW, Poli S. Experimentally based water budgets for dehydrating slabs and consequences for arc magma generation. Earth and Planetary Science Letters. 1998;163:361–379.

43. Schmidt MW, Poli S. Generation of mobile components during subduction of oceanic crust. In: Rudnick, R.L. (Ed.). Treatise on Geochemistry. The Crust. Elsevier Science Ltd. 2003;3:567–593.

44. You CF, Castillo PR, Gieskes JM, Chan, LH, Spivack AJ. Trace element behavior in hydrothermal experiments: İmplications for fluid processes at shallow depths in subduction zones. Earth and Planetary Science Letters. 1996;140:41–52.

45. Barnes I, O'Neil JR. The relationship between fluids in some fresh alpine-type ultramafics and possible modern serpentinization, western United States. Geological Society of America Bulletin. 1969;80(10):1947-1960.
Available:https://doi.org/10.1130/0016-7606(1969)80[1947:TRBFIS]2.0.CO;2

46. Moody JB. Serpentinization: A review. Lithos. 1976;9(2):25-138.
Available:http://dx.doi.org/10.1016/0024-4937(76)90030-X

47. Alt JC, Shanks III, WC. Stable isotope compositions of serpentinite seamounts in the Mariana forearc: Serpentinization processes, fluid sources and sulphur metasomatism. Earth and Planetary Science Letters. 2006;242:272–285.

Peer-review history:
The peer review history for this paper can be accessed here:
https://www.sdiarticle5.com/review-history/102253